

# Gamma Ray Bursts versus OB Associations: do they trigger star formation?

Yu. N. Efremov<sup>1</sup>, S. Ehlerová<sup>2</sup>, J. Palouš<sup>2</sup>

<sup>1</sup> Sternberg Astronomical Institute, MSU, Moscow 119899, Russia

<sup>2</sup> Astronomical Institute, Academy of Sciences of the Czech Republic, Boční II 1401, 141 31 Prague 4, Czech Republic

Received 11 March 1999/ Accepted 13 July 1999

**Abstract.** We discuss differences in shapes, expansion velocities and fragmentation times of structures created by an energy deposition from a single Gamma-Ray Burst (GRB) and an OB association to the ISM. After the initial inflation, supershells produced by GRBs are almost static or slowly expanding, contrary to more rapidly expanding supershells created by OB associations. We discuss the position of the energy source relative to the symmetry plane of the galaxy: observed arc-like structures can be the most dense part of structures formed by an expansion from a source above or below the galactic plane. Arcs may also form if the expansion takes place inside a giant HI cloud. We try to reproduce the size, the age, and the average distance between OB associations in the Sextant region at the edge of LMC 4.

**Stars: formation – ISM: bubbles – ISM: supernova remnants – Galaxies: individual: LMC – Galaxies: star clusters – Gamma rays: bursts**

## 1. Introduction

It is generally assumed that the HI shells and supershells observed in galaxies may be formed by the action of massive stars in OB associations or they may be created by impacts of high velocity clouds (HVC) into the galactic HI plane. Recently, another possibility has been proposed: they may result from an energy input connected with Gamma-Ray Burst (GRB) events. This may follow coalescence of two neutron stars in a binary system leading to the formation of a black hole. Such events, lasting a few milliseconds, release up to  $10^{54}$  erg of orbital kinetic energy of the progenitor. The energy may be released into a collimated jet illuminating only a fraction  $f_b$  of its sky. Such beaming would decrease the output

energy by a factor  $f_b$  and increase the frequency of occurrence by a factor  $f_b^{-1}$ . Another way to release several times  $10^{52}$  erg of energy is the collapse of a single super-massive ( $\geq 100M_\odot$ ) star, the hypernova (Paczynski 1998). X-ray afterglows, discovered by the satellite BeppoSAX, lasting several hours, result from the interaction between relativistic particles and the ambient medium around a black hole. The discovery of the host galaxies in the optical domain also points to an interaction between an energetic ( $10^{54}$  erg) event and the interstellar medium in galaxies (Kulkarni et al. 1998; Wijers 1998). Other evidence in favor of such superexplosions is given by Wang (1999), who discovered gaseous X-ray emitting remnants of two hypernovae in M101. Some cold HI shells may be the long lasting evidence of a short pulse of energy accompanying GRBs, as it has been noted by Blinnikov & Postnov (1998) and elaborated by Efremov et al. (1998) and Loeb & Perna (1998).

The intention of this paper is to demonstrate the difference between HI shells created in connection to GRBs and HI shells formed around OB associations. Properties of supershells created in connection with a GRB are determined by a single short-acting source of energy, which may arise in any position in a galaxy (and even outside it): the energy of  $10^{51} - 10^{54}$  erg is released in a few seconds from a very small volume of the accretion disk around the black hole. The activity of young stars in OB associations is much less concentrated in space and time: the initial volume can have a radius  $\geq 10$  pc and the energy may be delivered during several Myr. The duration of the energy supply depends in this case on the history of the star formation in the OB association and on the IMF, leading to a typical spread of 10 - 20 Myr.

In this paper we compare simulations of expanding shells connected with OB associations to those created by GRBs. We focus on the star formation around the LMC4 region in the Large Magellanic Cloud (LMC). Next we discuss arguments for and against the origin of multiple su-

Send offprint requests to: J. Palouš<sup>2</sup>

pershells from single superexplosion; and we consider the possibility that GRBs support star formation in galaxies.

## 2. Simulations of shells created by a GRB and by an OB association

The expansion of gas layers related to energy inputs from GRBs or OB associations can be described as a blast-wave propagating into the interstellar medium of the host galaxy (Ostriker & McKee 1988; Bisnovatyi-Kogan & Silich 1995). Since the radius of the shell is much larger than its thickness, the thin layer approximation developed by Sedov (1959) can be used. It has been applied in one-dimensional models by Chevalier (1974) and in two-dimensional models by Tenorio-Tagle & Palouš (1987) and Mac Low & McCray (1988). These models have been further extended into three dimensions by Palouš (1990) and Silich et al. (1996).

A system of equations of motion, mass, and energy is solved. The equation of motion is

$$\frac{d}{dt}(m_{sh}v_{sh}) = dS_{sh}[(P_{int} - P_{ext}) + \rho_{ext}v_{ext}(v_{exp} - v_{ext})] + m_{sh}g, \quad (1)$$

where  $m_{sh}$ ,  $v_{exp}$ ,  $dS_{sh}$  are the mass, the expansion velocity and the surface of an element of the shell,  $P_{int}$  and  $P_{ext}$  are pressures inside and outside the bubble,  $\rho_{ext}$  and  $v_{ext}$  are the density and velocity of the ambient medium, and  $g$  is the gravitational acceleration.

The equation of mass conservation is

$$\frac{d}{dt}m_{sh} = (v_{exp} - v_{ext})_{\perp}\rho_{ext}dS_{sh} - m_{sh}\Gamma_{sh}. \quad (2)$$

The first term on the right hand side (rhs), giving the increase of mass  $m_{sh}$ , is used as long as the normal component of the velocity,  $(v_{exp} - v_{ext})_{\perp}$ , exceeds the speed of sound in the ambient medium. After the expansion becomes subsonic, the mass accumulation stops. The second term on the rhs describes the decrease of mass in the shell due to mixing with the material inside the bubble;  $\Gamma_{sh}$  is the shell mixing rate.

The total energy  $E_{tot}$  is

$$E_{tot} = E_{pot} + E_{th} + E_{kin}, \quad (3)$$

where  $E_{pot}$  is the gravitational potential energy in the galaxy.  $E_{th}$  and  $E_{kin}$  are the thermal and kinetic energies:

$$E_{th} = E_{th,int} + E_{th,sh} + E_{th,ext}, \quad (4)$$

$$E_{kin} = E_{kin,int} + E_{kin,sh} + E_{kin,ext}, \quad (5)$$

where the second parts of the subscripts on the rhs refer respectively to the medium inside the bubble, in the shell, and in the unperturbed environment. In this paper,

we disregard the thermal energy of the unperturbed ambient medium  $E_{th,ext}$  and the kinetic energy of the medium inside and outside the bubble  $E_{kin,int}$  and  $E_{kin,ext}$ .

The balance of the internal thermal energy is given as

$$\frac{d}{dt}E_{th,int} = L - \Lambda_{int} + \Gamma_{sh}E_{th,sh}, \quad (6)$$

where  $L$  is the energy input rate from a GRB or an OB association and  $\Lambda_{int}(\rho_{int}, T_{int})$  is the radiative cooling rate from the bubble interior,  $\rho_{int}$  is the internal volume density,  $T_{int}$  is the internal temperature. For the mixing rate we assume

$$\Gamma_{sh} = \frac{f_{mix}}{t_{mix}}, \quad (7)$$

where

$$f_{mix} = \begin{cases} 1 & T_{int} < T_{sh} \\ 0 & T_{int} \geq T_{sh} \end{cases}, \quad (8)$$

$T_{sh}$  is the temperature in the shell. The mixing time  $t_{mix}$  is estimated as

$$t_{mix} = \frac{\alpha r_{sh}}{V_{sound,sh}}, \quad (9)$$

where  $r_{sh}$  is the radius of the shell and  $V_{sound,sh}$  is the sound speed inside the shell:  $V_{sound,sh} = \sqrt{\frac{kT_{sh}}{\mu}}$ ,  $k$  is the Boltzmann constant and  $\mu$  is the mean atomic weight of particles in the shell.  $\alpha$  is a free parameter giving the effectivity of the mixing process.  $\alpha$  lies in the interval  $(0, \infty)$ :

–  $\alpha = 0$  corresponds to an instantaneous mixing, all the mass collected in the shell is immediately mixed into the bubble

–  $\alpha = \infty$  corresponds to no mixing.

In our simulations we use  $\alpha$  in the range  $(0.1 - 1)$ , however results are almost independent on the particular value, and moreover, mixing has influence only on the early evolution of the supershell. It does not have a substantial influence on the later evolution after 1 Myr of expansion.

The balance equation of the thermal energy in the shell is

$$\frac{d}{dt}E_{th,sh} = \frac{1}{2} \frac{dm_{sh}}{dt}(v_{exp} - v_{ext})_{\perp}^2 - \Lambda_{sh} - \Gamma_{sh}E_{th,sh}, \quad (10)$$

where the first term on the rhs gives the fraction of the kinetic energy of the shell which is converted into the shell thermal energy due to the compression of the ambient medium.  $\Lambda_{sh}(\rho_{sh}, T_{sh})$  is the cooling rate of the shell, where  $\rho_{sh}$  is the volume density in the shell, which is estimated under the assumption that the thickness of the shell is a small fraction, ( $\sim 0.1$ ), of the shell radius.  $T_{int}$  and  $T_{sh}$  are derived from the thermal energies and number of particles in the bubble  $N_{int}$  and in the shell  $N_{sh}$ :  $T_{int} = \frac{E_{th,int}}{\frac{3}{2}kN_{int}}$  and  $T_{sh} = \frac{E_{th,sh}}{\frac{3}{2}kN_{sh}}$ . The radiative cooling

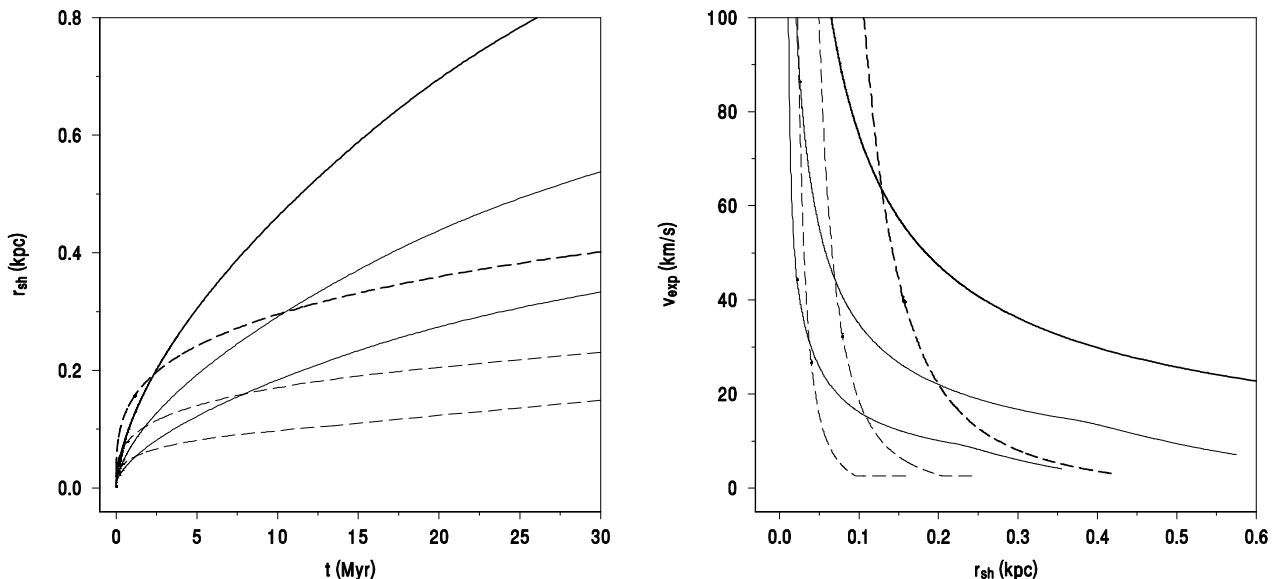


**Fig. 1.** The shell radius  $r_{sh}$  as a function of time (left panel) and the expansion velocity of the shell  $v_{exp}$  as a function of radius (right panel) for shells expanding in a homogeneous medium with  $\rho_{ext} = 1.4 \text{ cm}^{-3}$ . Solid lines denote the continuous energy input, the dashed ones the abrupt energy input. The thickness of the line gives the input energy, from thin to thick:  $10^{52}$ ,  $10^{53}$  and  $10^{54}$  erg.

rate from both the bubble and the shell is calculated using the cooling functions of Böhringer & Hensler (1989) for  $T \in (10^{3.5} - 10^8)$  K, and Schmutzler & Tscharnuter (1993) for  $T \in (10^8 - 10^9)$  K.

The internal pressure  $P_{int}$  is derived from the internal thermal energy  $E_{th,int}$  and the volume of the bubble  $V_{int}$

$$P_{int} = \frac{2}{3} \frac{E_{th,int}}{V_{int}}. \quad (11)$$

The distribution of the initial energy among the thermal and kinetic parts corresponds to the solution calculated by Sedov (1959), and the division of the initial thermal energy and mass between the internal volume and the shell is quite randomly chosen. However, different ratios of initial masses and energies do not influence results substantially.

The shell is split into elements in a 3D space, and equations of motion (1), mass (2), internal and shell thermal energy balance (6) and (10), and the equation for the internal pressure (11) are solved numerically using finite timesteps. To keep the accuracy of the integrated quantities under desired limits, an adaptive step-size control scheme is used.

The expansion in the static, homogeneous medium with  $\rho_{ext} = 1.4 \text{ cm}^{-3}$  is shown in Fig. 1. We compare results of the abrupt and continuous energy input of  $10^{52}$ ,  $10^{53}$ , and  $10^{54}$  erg:

- In the case of abrupt energy input, the shell rapidly expands to the radius of 50 - 150 pc during the first  $10^6$  yr. After 2 - 3 Myr the temperature  $T_{int}$  decreases below  $10^6$  K. The initial inflation is followed by a slower expansion at velocities  $v_{exp}$  close to the speed of sound in the ambient medium.
- In the case of continuous energy input, the growth of the radius is slower, reaching the size of 50 - 150 pc only after 2 - 3 Myr. There is rapid growth phase as in the previous case, however, the expansion velocity does not decrease as quickly. Already after 1 - 2 Myr it is higher than in the case of abrupt energy input.

After  $\sim 30$  Myr, shells reach diameters of 100 - 350 pc and 300 - 1000 pc and masses of  $10^{5.2} - 10^{7.1}$  and  $10^{6.9} - 10^{8.1} M_{\odot}$  for, respectively, abrupt and continuous energy inputs of  $10^{52} - 10^{54}$  erg. As seen in Fig. 1, shells connected to GRBs are smaller than shells connected to OB associations for most of the time. At diameters larger than 500 pc, GRB shells always expand at velocities below  $10 \text{ km s}^{-1}$ . Thus, large shells with diameters 500 - 2000 pc expanding at velocities 10 - 40  $\text{km s}^{-1}$  can not be created by an abrupt energy input connected to GRBs; they have to be created by a continuous energy input related to massive stars in OB associations.

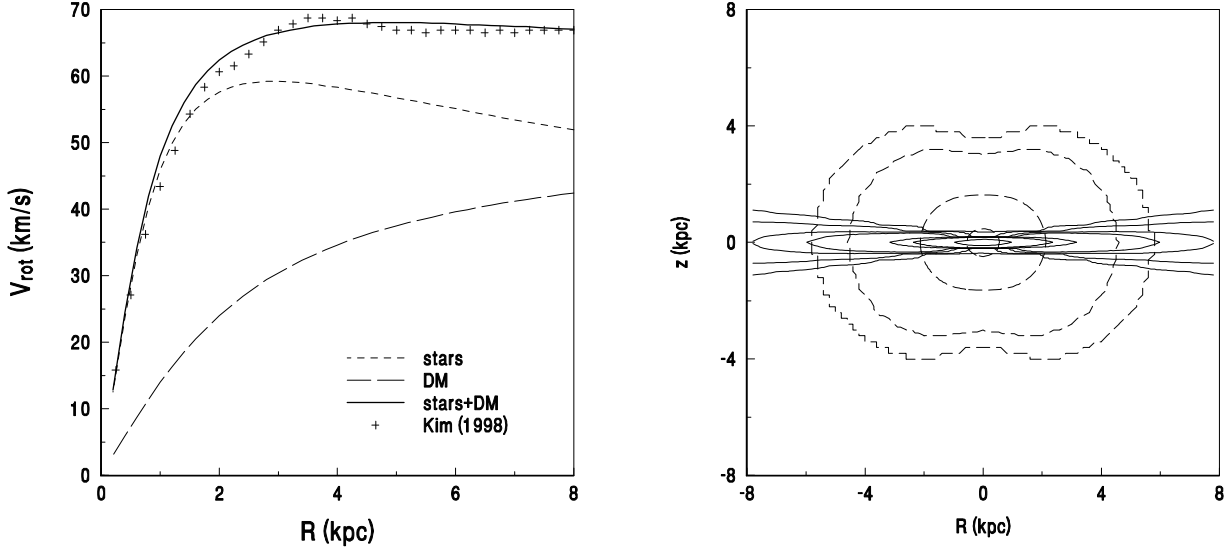


**Fig. 2.** Left panel: a comparison of the observed rotation curve with a model of the LMC composed of dark matter and stars. Right panel: the density distribution in a two component disk composed of cold gas - Solid line: (the values of the constant density are: 5.0, 1.0, 0.5, 0.1, 0.05, 0.01, 0.001  $\text{cm}^{-3}$ ) - supported almost completely by the centrifugal forces, and hot gas - Dashed line: (the values of the constant density are: 0.1, 0.01, 0.001, 0.0005  $\text{cm}^{-3}$ ) - balanced almost completely by pressure gradients.

### 3. Expanding shells in the LMC

In this section we apply the code described above to expanding shells in the Large Magellanic Cloud (LMC). For the LMC we propose a three component model composed of the interstellar medium, stars and dark matter. We assume that the large-scale shape of the gravitational potential is formed by stars and dark matter: the contribution of the ISM is neglected. The ISM contributes to local perturbations connected to instabilities and star formation.

#### 3.1. Stars and dark matter

The spherically symmetric volume density distribution of stars (subscript  $S$ ) is described by the Hubble-Reynolds profile

$$\rho_S(R) = \frac{\rho_{S,0}}{\left[1 + \left(\frac{R}{R_S}\right)^2\right]^{3/2}}, \quad (12)$$

and the less steep distribution of the dark matter (subscript  $DM$ ) with a function

$$\rho_{DM}(R) = \frac{\rho_{DM,0}}{1 + \left(\frac{R}{R_{DM}}\right)^2}, \quad (13)$$

where  $\rho$  is the volume mass density,  $R$  is the galactocentric distance.  $R_S$  is the core radius of the stellar distribution

and  $R_{DM}$  the radial scale length of the dark matter. The subscript 0 denotes values at the galactic center.

The stellar + dark mass within the radius  $R$  is

$$M_{S+DM}(R) = 4\pi R_S^3 \rho_{S,0} \times \left( \ln\left[\frac{R}{R_S} + \left(\frac{R^2}{R_S^2} + 1\right)^{0.5}\right] - \frac{R}{R_S} \left[\left(\frac{R}{R_S}\right)^2 + 1\right]^{-0.5} \right) + 4\pi R_{DM}^3 \rho_{DM,0} \left( \frac{R}{R_{DM}} - \arctan\left(\frac{R}{R_{DM}}\right) \right). \quad (14)$$

The galaxy extends up to the galactocentric distance  $R_B$ :

$$\rho = \rho_S + \rho_{DM} = 0 \quad \text{for} \quad R > R_B. \quad (15)$$

To balance the radial force a circular velocity  $V_{rot}(R)$  is required:

$$V_{rot}(R) = \left( \frac{GM_{S+DM}(R)}{R} \right)^{1/2}, \quad (16)$$

where  $G$  is the gravitational constant.

The potential is given as

$$\phi = -\frac{V_{rot}(R_B)^2}{2} F(R), \quad (17)$$

where

$$F(R) = 1 + \frac{1}{2} \frac{R_B}{R_{DM}} \frac{M_{DM}}{(M_{DM} + M_S)} \times$$

$$\begin{aligned}
& \left[ \ln\left(1 + \left(\frac{R_B}{R_{DM}}\right)^2\right) - \ln\left(1 + \left(\frac{R}{R_{DM}}\right)^2\right) \right] \\
& + \frac{R_B}{R_{DM}} \frac{M_{DM}}{(M_{DM} + M_S)} \left[ \frac{\arctan\left(\frac{R_B}{R_{DM}}\right)}{\frac{R_B}{R_{DM}}} - \frac{\arctan\left(\frac{R}{R_{DM}}\right)}{\frac{R}{R_{DM}}} \right] \\
& + \frac{R_B}{R_S} \frac{M_S}{(M_S + M_{DM})} \times \\
& \left[ \frac{\ln\left(\frac{R}{R_S} + \sqrt{1 + \left(\frac{R}{R_S}\right)^2}\right)}{\frac{R}{R_S}} - \frac{\ln\left(\frac{R_B}{R_S} + \sqrt{1 + \left(\frac{R_B}{R_S}\right)^2}\right)}{\frac{R_B}{R_S}} \right] \\
& \text{for } R \leq R_B \\
& F(R) = \frac{R_B}{R} \text{ for } R > R_B. \quad (18)
\end{aligned}$$

The rotation curve of the LMC given by Kim et al. (1998) is reproduced with  $R_S = 1$  kpc,  $R_{DM} = 2$  kpc,  $R_B = 8$  kpc, and the total mass  $M_{S+DM}(8 \text{ kpc}) = 8 \times 10^9 M_\odot$ . 60% of this mass is in stars and 40% in dark matter (see Fig. 2).

### 3.2. Interstellar medium

The interstellar medium is distributed in a two component disk, which is partially supported by the centrifugal force and partially balanced by the pressure gradients:

$$V_G(r) = \left( e^2 r \frac{\partial \phi}{\partial r} \right)^{1/2}, \quad (19)$$

where  $V_G$  is the plane parallel rotational velocity of the gas at a distance  $r$  from the rotational axis. A fraction  $e^2$  of the gravitational force  $\frac{\partial \phi}{\partial r}$  towards the rotational axis is balanced by the centrifugal force, the complementary fraction  $(1 - e^2)$  is balanced by the pressure gradients.  $e$  is a free parameter from the interval  $0 < e < 1$ :  $e = 1$  means that the gravity is completely balanced by the centrifugal force,  $e = 0$  means that the gravity is completely balanced by pressure gradients. This model has been described by Tomisaka & Ikeuchi (1988) and used by Suchkov et al. (1994) and Silich & Tenorio-Tagle (1998) for models of large-scale bipolar flows from nuclear starburst in dwarf galaxies.

The distribution of the gas is given as

$$\rho_G = \rho_{cold} + \rho_{hot}, \quad (20)$$

with

$$\rho_i = \rho_{i,0} \exp(const_i \chi), \quad (21)$$

where  $i$  stands for *cold* or *hot* gaseous components.  $const_i$  is inversely proportional to the square of the sound speed  $c_S$  and to the temperature  $T$  of the gaseous component, and

$$\chi = \phi(R) - e^2 \phi(r) - (1 - e^2) \phi(0). \quad (22)$$

The cold and hot gaseous components vary in the degree of pressure support:

- the cold component, where we assume  $c_S = 8 \text{ km s}^{-1}$  (corresponding to  $T = 10^4 \text{ K}$ ), is distributed in a disc mainly supported by its rotation:  $e = 0.9$ ;
- the hot component, where  $T = 10^6 \text{ K}$ , is more supported by pressure gradients:  $e = 0.5$ , resulting in an almost spherical distribution.

Densities of both components in a model of the LMC are shown in Fig. (2). With  $\rho_{cold,0} = 11 \text{ cm}^{-3}$  and  $\rho_{hot,0} = 0.15 \text{ cm}^{-3}$ , the total mass of the cold and hot component within 4 kpc is  $5.2 \times 10^8 M_\odot$ , respectively  $5.2 \times 10^7 M_\odot$ .

### 3.3. Fragmentation of expanding shells

Conditions for the instability and fragmentation of expanding decelerating shells have been expressed by Ehlerová et al. (1997) using results of the linear perturbation theory of transverse motions on a three-dimensional shell expanding into a uniform ambient medium, as discussed by Elmegreen (1994) and Vishniac (1994). The stretching of the perturbed region due to the expansion may be compensated by the convergence of the flow due to the self-gravity of the shell, if the maximum growth rate of a transverse perturbation  $\omega > 0$ .

$$\omega = -\frac{3v_{exp}}{r_{sh}} + \sqrt{\frac{v_{exp}^2}{r_{sh}^2} + \left(\frac{\pi G \Sigma}{c}\right)^2}, \quad (23)$$

where  $\Sigma$  is the mass column density of the shell,  $c$  is the speed of sound within the shell. The wavelength of the fastest transversal perturbation,  $\lambda$ , is given as

$$\lambda = \frac{2c^2}{G\Sigma}. \quad (24)$$

$\omega$  and  $\lambda$  can be evaluated in 3D computer simulations using the thin shell approximation. In the beginning of an expansion, when  $v_{exp}$  is large and  $r_{sh}$  is small,  $\omega$  is always negative, and the shell is stable. The stretching because of the rapid expansion at early stages is much more important than the self-gravity of the shell. Later,  $v_{exp}$  decreases and  $r_{sh}$  increases, so that the first negative term in Eq. (23) becomes less important, and at the same time  $\Sigma$  increases so that the second term in Eq. (23), which is always positive, becomes more important. At the expansion time  $t_b$ ,  $\omega$  becomes positive and we start to evaluate the fragmentation integral  $I_f(t)$ :

$$I_f(t) = \int_{t_b}^t \omega(t') dt'. \quad (25)$$

At the time  $t = t_f$  when  $I_f(t) = 1$ , fragments are already well developed. We also calculate the wavelength  $\lambda$  at the times  $t_b$  and  $t_f$ .

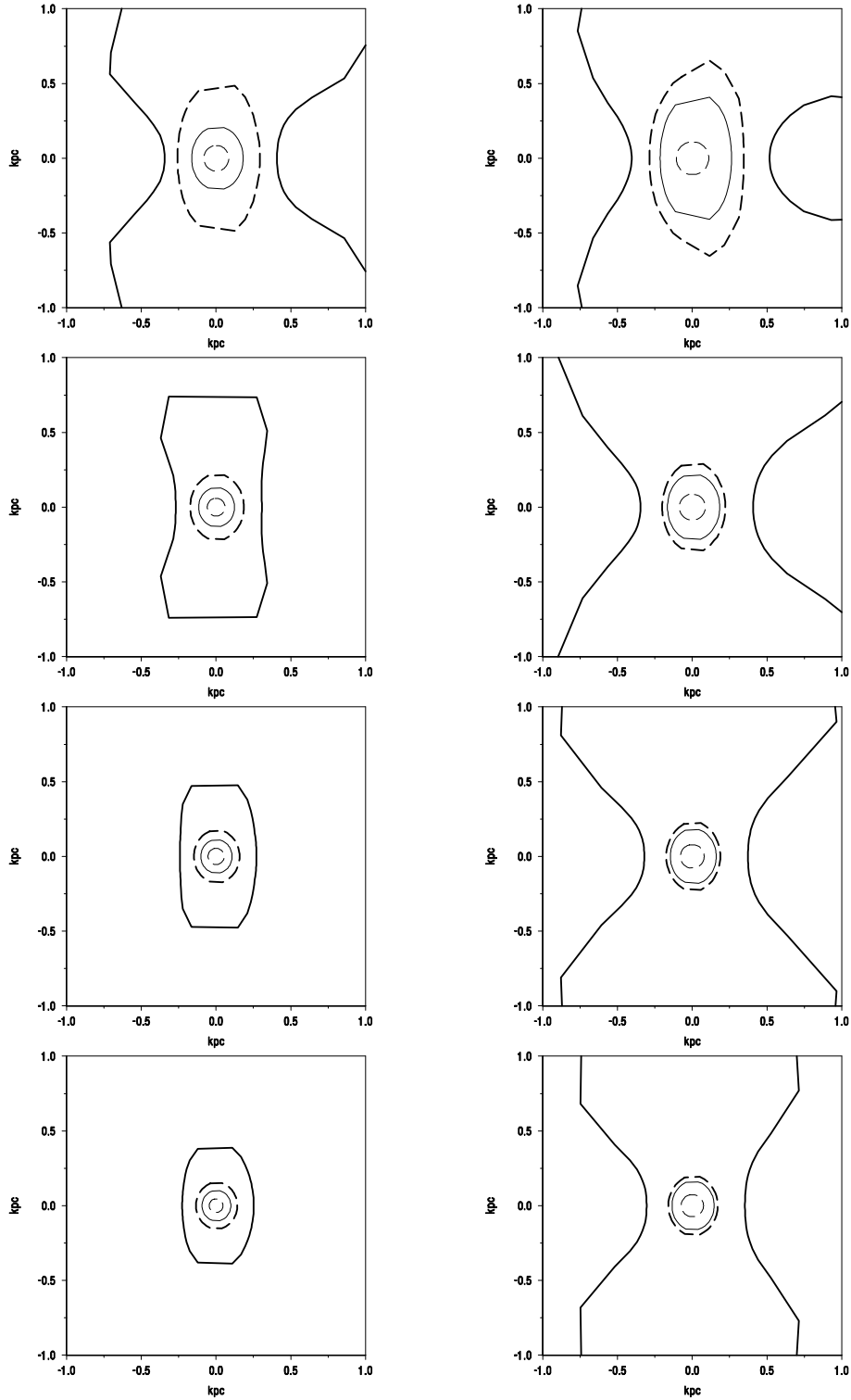


**Fig. 3.**  $R - z$  cuts of expanding shells at a distance of 2 kpc from the center of the LMC after 10 Myr (left panel) and 20 Myr (right panel) of evolution. The galactic center is in the direction to the left of the (0, 0) point. The density of the ambient medium  $\rho_{ext}(z = 0)$  from the upper to the bottom row is: 1.4, 10, 20, 30  $\text{cm}^{-3}$ . Thin and thick lines correspond to an input energy of  $10^{52}$  and  $10^{54}$  erg respectively, solid and dashed lines mean a continuous or abrupt energy input.

$\rho_{ext}$ $cm^{-3}$	type	$E_0$ erg	$r_{ini}$ pc	$t_b$ Myr	$r(t_b)$ pc	$\lambda(t_b)$ pc	$t_f$ Myr	$r(t_f)$ pc	$\lambda(t_f)$ pc
1.4	GRB	$10^{52}$	4						
	GRB	$10^{53}$	9						
	GRB	$10^{54}$	20	8.8	252	99	32	632	14
	SN	$10^{52}$	2	17	207	121	> 35		
	SN	$10^{53}$	2	13	276	83	35	348	105
	SN	$10^{54}$	2	9.1	334	64	23	413	59
10	GRB	$10^{52}$	2						
	GRB	$10^{53}$	5	5.4	86	48	26	128	86
	GRB	$10^{54}$	10	3.7	133	30	11	175	22
	SN	$10^{52}$	1	8.9	110	37	18	159	24
	SN	$10^{53}$	1	6.6	145	27	13	210	17
	SN	$10^{54}$	1	4.7	186	20	9.5	264	13
20	GRB	$10^{52}$	2						
	GRB	$10^{53}$	4	3.7	67	31	15.5	100	44
	GRB	$10^{54}$	8	2.5	102	20	7.2	136	14
	SN	$10^{52}$	1	6.5	80	26	13	119	17
	SN	$10^{53}$	1	4.9	107	19	9.7	157	12
	SN	$10^{54}$	1	3.5	138	14	7.0	202	9
30	GRB	$10^{52}$	2						
	GRB	$10^{53}$	3	3.0	57	25	10.0	79	27
	GRB	$10^{54}$	7	2.0	88	16	5.8	117	11
	SN	$10^{52}$	1	5.4	67	21	11	99	14
	SN	$10^{53}$	1	4.0	89	15	8.1	132	10
	SN	$10^{54}$	1	2.9	115	12	5.9	171	7

**Table 1.** 3D simulations of expanding shells in the model of the LMC.  $\rho_{ext}$  is the density of the ambient medium at  $R_0 = 2$  kpc,  $z = 0$  kpc. The value  $1.4 \text{ cm}^{-3}$  corresponds to the described model, other values are artificially increased. GRB means an abrupt energy input, SN a continuous one.

### 3.4. Expanding shells

We have done computer simulations listed in Table 1. The value of  $\rho_{ext} = 1.4 \text{ cm}^{-3}$  corresponds to the density at a distance of 2 kpc from the center of the LMC (and  $z = 0$ ). We calculated experiments with higher densities of the ambient medium, too. The density could be locally increased as a result of sweeping of the mass from other places.

Due to gradients of the ISM density and to the form of the gravitational potential, shapes of expanding shells are not spherical; they are usually elongated in the direction perpendicular to the galaxy plane. This is demonstrated in the  $R - z$  cuts through expanding shells, which are shown after 10 and 20 Myr of expansion in Fig. 3. For the continuous energy input only the low energy cases,  $E_0 = 10^{52}$  erg, do not blow-out to the galactic halo. For  $E_0 \geq 10^{53}$  erg bubbles blow-out to high  $z$  distances. With the low (not enhanced) value of the density of the ambient medium, the blow-out is radially asymmetrical, as can be seen in Fig. 3. This radial asymmetry is the result of gradients in the distribution of the hot gaseous component, which produce the outflow in the direction away from the galactic center, as seen at high  $z$ -distances in Fig. 3. This effect may result in a systematic difference between observed shapes of supershells at the near and far side of the LMC: they should be more round in the north-eastern part

of the LMC than in the south-western one (for the discussion of the LMC spatial orientation see Sect. 4). As an example the nearly circular supergiant shell SG24 in the NE and the elliptical shell SG8 in the SW can be given (Kim 1998). The abrupt energy input creates much less asymmetrical bubbles, which even for higher energies do not blow-out to the galactic halo. These shells stay near the galaxy plane even for the highest input energies and lowest external densities; they never reach the height of 1 kpc from the  $z = 0$  plane. This is a more general result, connected to the initial rapid expansion and subsequent decrease of the shell expansion velocity for the abrupt energy input. GRB can lead to a blowout if they explode below or above the symmetry plane of the galaxy, or if they release high energies ( $\sim 10^{54}$  erg) in thin-disk spiral galaxies.

In Table 1 we give fragmentation times  $t_b$  and  $t_f$  and wavelengths of the fastest perturbation,  $\lambda$ , given by Eq. (24). We add simulations with low input energy,  $E_0 = 10^{51}$  erg, corresponding to the energy of one supernova. For this input, energy shells are small and always stable for any tested density. It means that an isolated SN explosion or GRB of the same energy can not induce gravitational fragmentation and trigger star formation. To do so in the LMC (and elsewhere) higher input energies are needed.

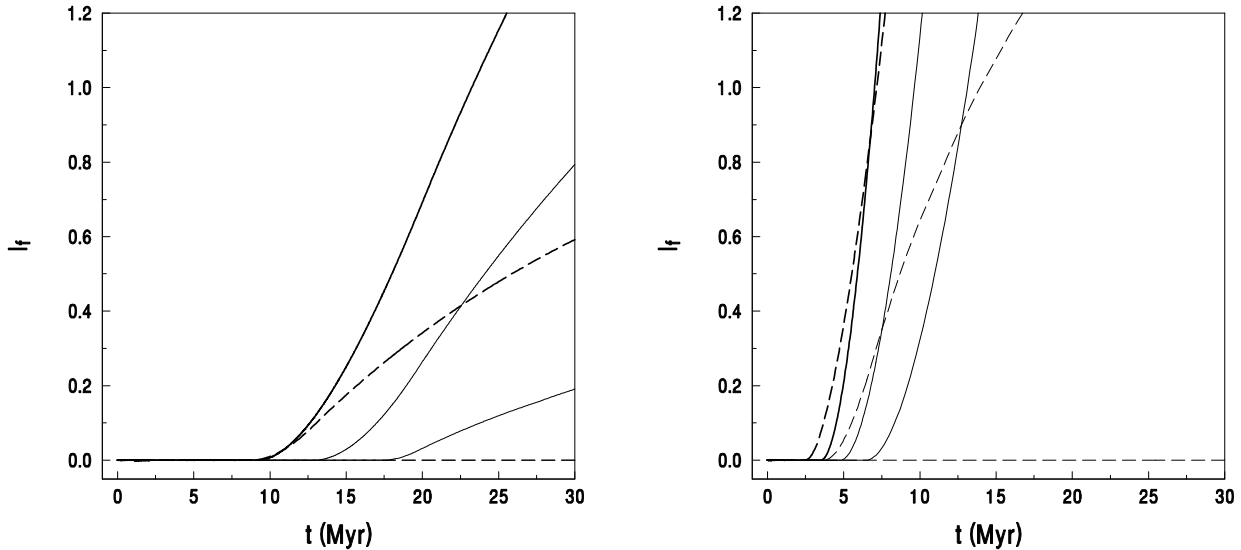


**Fig. 4.** The fragmentation integral  $I_f$  as a function of time for  $\rho_{ext} = 1.4 \text{ cm}^{-3}$  (left panel) and  $\rho_{ext} = 20 \text{ cm}^{-3}$  (right panel). Designation of lines is the same as in Fig. 1.

Shells related to continuous energy inputs can fragment for lower input energies than shells created by abrupt ones: in the first case  $E_0 \geq 10^{52}$  erg is enough for a density of the ambient medium in the range  $\rho_{ext} = 1 - 30 \text{ cm}^{-3}$ . In the second case  $E_0 \geq 10^{53}$  erg is needed for  $\rho_{ext} \geq 10 \text{ cm}^{-3}$ , and  $E_0 \geq 10^{54}$  for  $\rho_{ext} = 1.4 \text{ cm}^{-3}$ .

The time evolution of the fragmentation integral  $I_f$  is shown in Fig. 4. In the low density ambient medium shells are stable for quite a long time. Except for the continuous input of  $10^{54}$  erg, neither of the cases reaches  $t_f$  before 30 Myr, which means, that the fragmentation is very slow if it happens at all.

For higher values of the density of the ambient medium, the shells fragment. For input energies  $E_0 \geq 10^{53}$  erg, the instability starts earlier for abrupt energy input cases, but it proceeds faster in continuous cases than in their abrupt counterparts.

#### 4. Triggered star formation at the edge of LMC 4 in the Sextant region

In this section we focus on a region in the LMC near Shapley's Constellation III, where several OB associations have been identified by Lucke & Hodge (1970). A supergiant HI shell surrounding the most prominent HI void in the LMC can be seen in e. g. Kim et al. (1998) at the same location. At the SW edge of this shell, outside the HI void, OB associations LH51, LH54, LH60w, LH60e, and LH63 form a fraction of the arc. This arc has been named the Sextant

by Efremov & Elmegreen (1998a), since the OB stars make about 1/6 of the complete circle. Its radius is estimated to be  $\sim 170$  pc and the average distance between subsequent OB associations in the arc is  $\sim 32$  pc. Near the center of the Sextant, two star clusters (HS288 and HS287) have been found. The oldest stars in the Sextant are  $\sim 7$  Myr old. We assume the age of the two star clusters to be 10 - 15 Myr. The direct determination of ages of these clusters is desirable.

Here, we would like to discuss once more the scenario proposed by Efremov & Elmegreen (1998a), i.e. that  $\sim 15$  Myr ago the energy has been released from star clusters HS288 and HS287 and formed an expanding shell. Later, the shell fragmented and triggered the formation of OB associations, which during the following 7 Myr moved to the presently observed configuration, the Sextant. An alternative concept is the energy injection from a merging event between two compact components of the close binary system related to a GRB: the progenitor was probably ejected from the nearby massive star cluster NGC 1978 (Efremov 1998, 1999a; Efremov & Elmegreen, 1998b) as a consequence of SN explosions leading to the formation of compact components. If this is the case, HS287 and HS288 have nothing to do with the Sextant. It may explain why the two clusters are slightly off center with respect to the Sextant arc. Some questions remain unanswered in both scenarios: particularly, why we see only a fraction of the

circle, and how its orientation relative to the line of nodes of the LMC (see below) may be explained.

We try to reproduce the shape of the Sextant, its radius, age and the distances between the OB associations using numerical simulations of shells expanding in a model of the LMC, taking into account different positions relative to the symmetry plane. An alternative scenario is the supershell expanding in the preexisting HI supercloud, which may be a result of the gravitational fragmentation in walls of the HI ring surrounding the LMC 4 region.

The position of the LMC on the sky is specified by the line of nodes  $\theta_0$  and the inclination  $i$ . We adopt values given by Luks & Rohlfs (1992):  $\theta_0 = 162^\circ$ ,  $i = 33^\circ$ . An analysis of proper motions of LMC stars in the Hipparcos catalogue revealed (Kroupa & Bastian 1997), that the LMC rotates clockwise. In the combination with the analysis of radial velocities by Luks & Rohlfs (1992) it means, that the SW half is the more distant part of the LMC and the NE half is the nearby one.

The Sextant itself is almost perpendicular to the line of nodes with the radius parallel to it. It is also interesting, that a continuation of the Sextant arc would cross the LMC 4 HI ring nearly perpendicularly. Therefore, its radius of 170 pc is almost uninfluenced by projection effects, while the deprojected average distance between the OB associations in the Sextant is  $l_{OB} \sim 37$  pc.

Using computer simulations, we search for such initial energies and densities of the ambient medium to get unstable shells with radii of 170 pc. With a shell of radius 170 pc we ask what was the value of the fragmentation integral  $I_f(t)$  some 7 Myr ago (7 Myr is the age of the oldest stars in the Sextant). We request a value between 0 and 1. For small values of  $I_f$  (near 0) the formation of stars must have been a very quick process, since they formed very shortly after the shell started to be unstable. For  $I_f$  near 1 the star formation was somewhat delayed. If  $I_f = 0$  about 7 Myr before reaching the radius 170 pc, shells do not fragment early enough and cannot form OB stars in the Sextant. If  $I_f > 1$  7 Myr before reaching 170 pc, shells also cannot reproduce the Sextant, since stars would probably form earlier and the observed arc of OB associations would be composed of older stars.

We ask what is the ratio between the wavelength of the fastest transversal perturbation in the shell,  $\lambda$ , and the shell radius  $r_{sh}$  7 Myr before reaching the radius of 170 pc. In our opinion, this value did not change since the formation of the first stars. Therefore, it should reproduce the presently observed ratio of the average deprojected distance between the OB associations  $l_{OB}$  to the radius of the Sextant:  $\frac{37}{170} = 0.22$ .

The above conditions restrict the possible values of the input energy and of the density of the ambient medium:

- The continuous energy input forms shells of a nearly correct size for  $E_0 = 10^{53}$  erg and  $\rho_{ext} = 20 \text{ cm}^{-3}$ : at  $t = 4$  Myr  $r_{sh} = 105$  pc,  $I_f = 0.1$ , and  $\lambda/r_{sh} = 0.18$ . The radius of 170 pc is reached 11 Myr after the

beginning of the expansion. Other simulations do not meet the conditions so well.

- The abrupt energy input gives the best solution with  $E_0 = 10^{54}$  erg and  $\rho_{ext} = 10 \text{ cm}^{-3}$ . At  $t = 3$  Myr  $r_{sh} = 130$  pc,  $I_f = 0.1$ , and  $\lambda/r_{sh} = 0.22$ . The radius 170 pc is reached at  $t = 10$  Myr. Lower energies or higher densities do not fulfill the above conditions.

We conclude, that for both continuous and abrupt energy input we can reproduce the correct size, age and average distance between fragments, observed in the Sextant. The continuous energy input gives the best solution for an input energy of  $10^{53}$  erg and density of the ambient medium  $20 \text{ cm}^{-3}$ . In the case of abrupt energy input, a higher value of energy ( $10^{54}$  erg) and a lower density of the ambient medium ( $\sim 10 \text{ cm}^{-3}$ ) are needed.

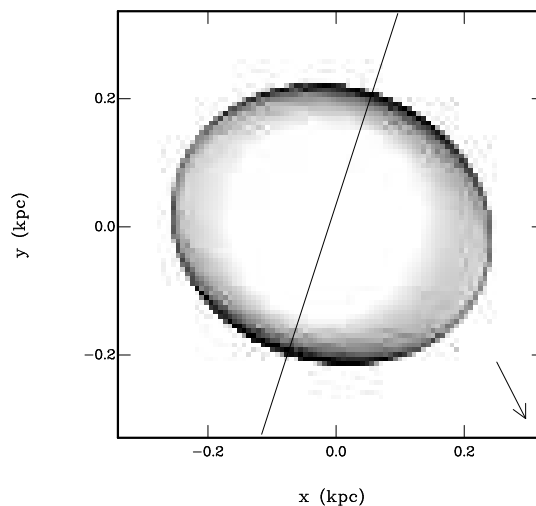


**Fig. 5.** Projected column density of an expanding shell created by the continuous energy input from the expansion center at the symmetry plane of the galaxy. North is up and West is right, the line shows the direction of the line of nodes, the 100 pc long arrow points towards the center of the LMC.

We try to reproduce not only the size of the shell at the right time and distances between fragments, but we would like to have the correct orientation in the LMC and give plausible arguments why the Sextant is only a fraction of the total circle. Here, projection effects play a role. In Fig. 5 we show the column density in the shell with the continuous input energy source of  $10^{53}$  erg in the symmetry plane of the galaxy at  $t = 11$  Myr,  $\rho_{ext}(z = 0) = 20 \text{ cm}^{-3}$ . The galaxy plane is observed in such a position that the line of nodes  $\theta_0 = 162^\circ$  and the inclination  $i = 33^\circ$ . The column density is distributed in an elliptical ring. Its ellipticity corresponds to projected dimensions of the 3D egg-shaped shell (see R-z cuts in Fig. 3), not to the

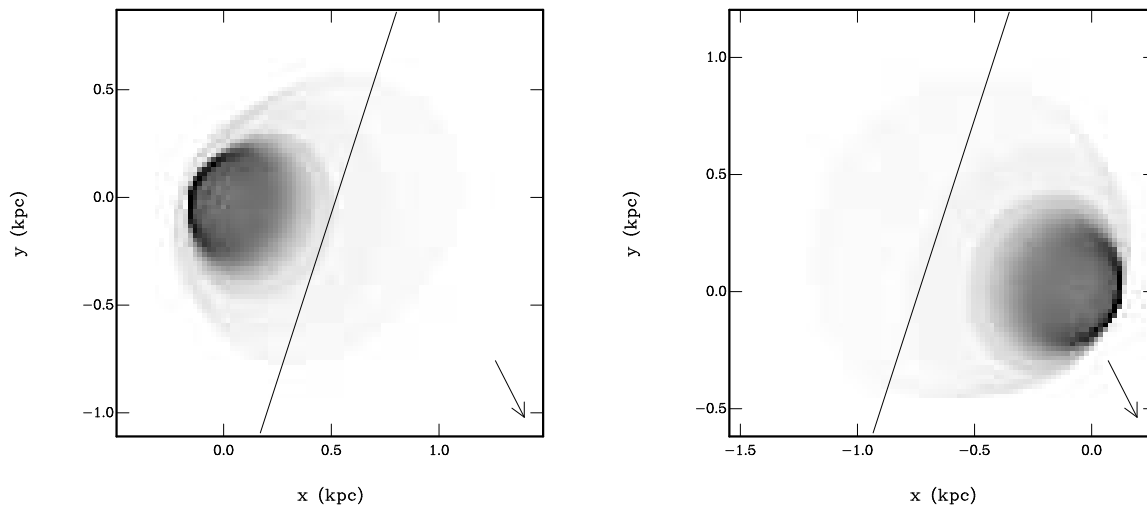


**Fig. 6.** The projected column density of a shell expanding from  $z = 100$  pc above (left panel) or  $z = -100$  pc below (right panel) the symmetry plane of the galaxy. North is up and West is right, the line shows the direction of the line of nodes, the 300 pc long arrow points towards the center of the LMC.

cosine of the inclination angle as would be the case of the projection of the in-plane ring. There are two maxima in the column density resulting from projection effects. They correspond to those directions where the path along the line of sight in the shell is long. Minima appear where the line of sight intersects the shell almost perpendicularly.

To get one-sided structures with one maximum in the column density, we calculated models with sources at different distances above or below the galactic plane. In Fig. 6 we show two cases with a continuous energy source of  $10^{53}$  erg placed at  $z = 100$  pc and  $z = -100$  pc,  $\rho_{ext}(z = 0) = 20 \text{ cm}^{-3}$ . The expanding structure is asymmetrical because of the asymmetry in the density distribution and the gravitational potential. Its most dense part is at low  $|z|$  distances near the symmetry plane and its low density parts open to high  $|z|$  distances. The projected column density shown in Fig. 6 has one maximum and it has the shape of an arc. However, the orientation and opening of the arc is in both cases (with the source above or below the symmetry plane) different from the observed position of the Sextant.

At the edge of LMC 4 the HI density may have been increased by sweeping of the mass from the HI void as observed by Kim et al. (1998). The HI collected there probably fragmented and formed giant clouds of increased HI density. We assume that the source of energy resided inside one of such HI clouds. In Fig. 7 we show results of a simulation where the shell formed around a continuous energy source. The expansion started in a homogeneous spherical cloud of density  $20 \text{ cm}^{-3}$  and radius 150 pc, where the energy source has been placed at an off-center position

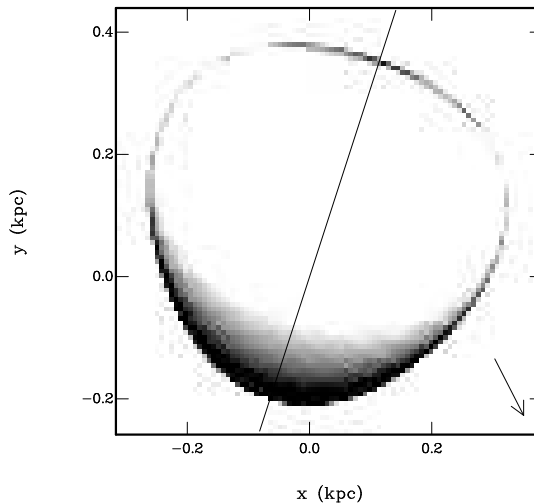


**Fig. 7.** The projected column density of a shell expanding from an off-center position inside a preexisting HI giant cloud. North is up and West is right, the line shows the direction of the line of nodes, the 100 pc long arrow points towards the center of the LMC.

(about 50 pc from the cloud center). The resulting projected column density (Fig.7) does not depend strongly on the position of the source inside the parent cloud. The energy sources inside a rather large area NW from the giant cloud center produce the shape and orientation in

the LMC similar to the Sextant. This is shown in Fig. 8, where the model projected column density is plotted over the photographic image of the Sextant area.

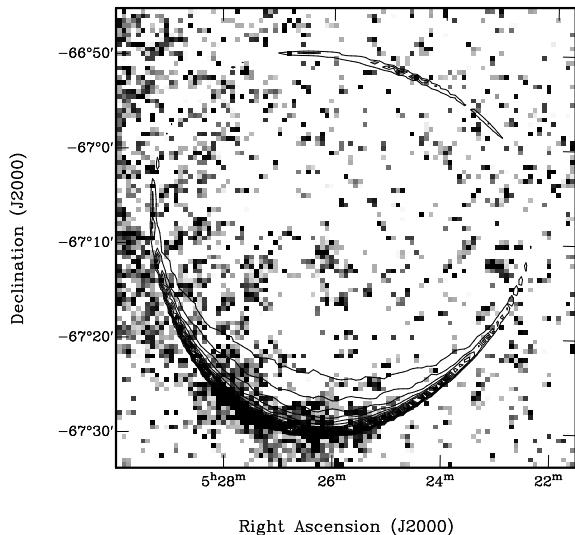


**Fig. 8.** A part of the photographic image of the Constellation III region including the Sextant arc. The original photograph from Boyden Observatory, courtesy of Harlow Shapley, Harvard College Observatory, has been put to computer readable form by Knut Olsen, Paul Hodge and Don Brownlee. The photographic image is overlaid with isodensity lines giving the model column density (the maximum projected column density is  $4.2 \times 10^{20} \text{ cm}^{-2}$ , lines show 90% , 80% ... 10% of this value).

We conclude that shell forming a fraction of the complete circle in the correct position can be created by expansion which takes place in the NW part of a preexisting giant HI cloud at the edge of LMC 4.

### 5. Can GRB trigger and support star formation in galaxies?

We have demonstrated that the abrupt energy inputs related to GRBs form expanding shells, which can fragment and trigger star formation. An inspection of Table 1 shows that with energy  $E_0 = 10^{54}$  erg shells fragment in any tested density of the ambient medium:  $\rho_{ext} = 1 - 30 \text{ cm}^{-3}$ . In our opinion, GRB are the likely cause of the supershell and the triggering of star formation, particularly when:

1. there is no stellar cluster inside a supershell or inside an arc of young OB stars (providing the normal IMF),
2. there is no evidence of HVC and/or neighbouring galaxies,
3. there is no hot gas inside the shell, even in the case of a young supershell,

4. there is a system of multiple stellar arcs.

The hypothesis of Blitz et al. (1999), that HVCs are debris after formation of the Local group of galaxies, suggests large distances to HVCs, which imply for a HVC the typical mass of  $3 \times 10^8 M_\odot$  of neutral gas and the typical size of 25 kpc. In such a case the theory, that the largest superbubbles may be created by impacts of HVCs, seems to be less plausible.

Many supershells in M31 (Brinks & Bajaja 1986) and M33 (Deul & den Hartog 1990) have a circular form and there are no visible OB associations inside them. A number of supergiant shells without visible clusters is known in isolated galaxies, where the probability of HVC infalls is low, for example galaxies NGC 3044 and NGC 4631 (see references in EfreMOV et al. 1998 and Loeb & Perna 1998).

Recently, a special photometric search for clusters, which could be the energy source of the supershells in the irregular dwarf galaxy Holmberg II, was carried out by Rhode et al. (1999). They found only 4 out of 50 supershells with clusters of suitable ages, which could have contained enough OB stars to form the observed supershells, assuming the normal IMF. The best examples of supershells with no clusters are the most energetic ones found in the low density environment at the periphery of Ho II, where no star formation occurs and where the presence of massive clusters is almost excluded. Another result given by Rhode et al. (1999) is that nearly no HVCs exist around Ho II, which may eventually be responsible for the observed supershells. Hypernovae are also not the likely energy source, since they reside near the star forming regions (Paczynski, 1998), and there is no star formation near the supershells at the periphery of Ho II. The energy source could be a merging event of a compact binary system. Supernova explosions, leading to the formation of compact components, may give the system the high space velocity of  $\geq 100 \text{ km s}^{-1}$  (Blaauw 1961). Then, the GRB occurs far from the formation site as demonstrated e.g. by Lipunov et al. (1997).

The Sextant arc is one in the system of three stellar arcs in the LMC 4 region (Hodge 1967, EfreMOV & Elmegreen 1998a). If the GRB theory of the origin is correct, then the progenitor of the Sextant arc (and progenitors of the other arcs as well) probably belonged to the massive 2 Gyr old cluster NGC 1978 located 0.5 - 1.0 kpc from its center. NGC 1978 has an elongated shape which may be the result of merging of two clusters, or of disk-shocking. Such events are able to eject many stars (including compact binaries) from the cluster. Actually, there is concentration of X-ray binaries in the discussed region. Also, one probable relict of the merging event of the compact binary system, the Soft Gamma Repeater SGR 0526-66 in SNR N49, is at a distance of 18' from the cluster NGC 1978 (EfreMOV 1998, 1999a, b).

At least three systems of multiple stellar arcs are known in the LMC, NGC 6946 and M 83 (Hodge 1967; EfreMOV 1999a). The opening angle in most of these arcs

is few dozen degrees. The strictly circular form of these arcs implies an origin from the central source. Regular distances between clusters along an arc suggest their formation by the gravitational instability in the swept-up gas ring (Sextant and two arcs in M 83).

Many questions related to the origin of supershells and triggered star formation in connection to GRBs remain open:

- Can isolated galaxies with active star formation be those in which there were recently many GRBs?
- Can GRBs support and revive star formation activity together with OB stars and SNe?
- Can GRBs be the initial source to the star formation and turbulent motions in gas disks of galaxies?

The last item (Hodge 1998, private communication) is quite attractive: compact binaries with neutron stars may form in the process of dynamical evolution of massive and old star clusters. The two compact components merge and produce GRBs long after they escaped from the cluster. Those, which explode within the gas disk, might trigger the turbulent motions and star formation there.

Considering the large uncertainties in the theory of GRBs, properties of supershells and stellar arcs suggested to be created by GRBs may give essential constraints to the GRB theory. The central angle of stellar arcs, for example, may be connected somehow with the beam angle of the GRB - especially if they cannot be explained as projected shells created by sources outside the galaxy plane or by sources inside giant interstellar clouds.

Our simulations show one possible obstacle to GRBs playing an active role in star formation events in galaxies. The energy needed to create gravitationally unstable shells by an abrupt explosion must be very high ( $E_0 \geq 10^{53}$  erg; for low ISM densities even  $E_0 \geq 10^{54}$  erg). There were indeed GRBs with energy  $10^{53}$  and  $10^{54}$  erg, such as GRB 971214 and GRB 990123 (Kulkarni et al. 1999), but the beaming of the relativistic jets would imply that the emitted energy would be proportionally smaller. So, if the energy loss during the time interval between the burst itself and the time when the expanding shock forms, is large, or if the energy released by the burst is small, then the effect of GRBs on the host galaxy is minor and it can not induce star formation.

## 6. Conclusions

We discussed properties of HI shells connected either to GRBs or OB associations: in the first case, there is an initial inflation or rapid growth of the shell followed by a slow expansion. In the second case the initial expansion is much slower, however, the expansion velocity decelerates to low values longer. Supershells of diameters larger than 500 pc are almost static if related to GRBs. If a supershell larger than 500 pc expands with a velocity higher than  $\sim 10 \text{ km s}^{-1}$ , it is undoubtedly related to an OB association (= continuous energy input).

Using computer simulations of expanding shells in galaxies, we showed that both the abrupt energy input connected to a GRB or a continuous energy input connected to an OB association can trigger star formation. Shells related to GRBs need the higher energy to fragment into protoclusters than shells connected to OB associations, where the lower energy is sufficient. The star formation triggered by GRBs can initiate or complement the star formation triggered by OB associations.

As an example, we discussed the Sextant region in the vicinity of LMC 4. This arc of OB associations can be interpreted as triggered star formation within the HI shell. We found that both abrupt and continuous energy inputs can correctly reproduce the radius, the age of the arc and the average distance between OB associations.

Partial shells formed by an energy source above or below the galactic plane are projected to the tangential plane perpendicular to the line of sight as arcs with apexes turned to or from the line of nodes of the LMC. This is not the case with the arcs in the LMC 4 region. To reproduce the orientation and position of the Sextant we have to assume, that the expansion took place inside a giant HI supercloud, which had been previously formed at the rim of LMC 4.

Clusters HS287 and HS288 are not in the very center of the Sextant arc. This may be explained as a consequence of the asymmetry of the shell: the projected structure (or its densest parts) has a center at a position different from the energy source.

A comparatively large number of SNe is needed to fit the observed arc. A cluster producing 10 - 100 SN requires, with the normal IMF, many low-mass stars in the same cluster. Unfortunately, there is no photometry for these clusters available to check their mass function. Because of the proximity of the massive star cluster NGC 1978, there is a high probability that both compact binaries and hypernovae exist in this region (e.g. Chevalier & Li 1999). The occurrence of very massive clusters near the arc systems in LMC and NGC 6946 shows that their progenitors may be stellar objects.

In any case, the presence of two or three more arcs composed of OB stars and clusters in the same region near LMC 4 (Efremov & Elmegreen 1998a), and the absence of similar arcs elsewhere in the LMC, can be better explained by a number of progenitors escaping from a single massive cluster, presumably NGC 1978. The recent discovery of the most massive young cluster in the galaxy NGC 6946, which is located near the only multiple arc system in this galaxy (Hodge 1967; Larsen & Richtler 1999), supports the idea of the connection between multiple, not concentric arcs with progenitors escaping from one common massive cluster.

*Acknowledgements.* We would like to thank Bruce Elmegreen and Guillermo Tenorio-Tagle for careful reading of the paper and the anonymous referee for valuable comments. We are

grateful to Sungeun Kim for the full text of her PhD thesis devoted to the high-resolution HI observation of the LMC and for providing us with the HI total column density map of the LMC. Yu. N. E. appreciates the partial support by the Russian Foundation of Fundamental Researches and the Council for the Support of Scientific Schools. He is also sincerely grateful to Jan Palouš and to the staff of the Astronomical Institute of the Academy of Sciences of the Czech Republic for warm hospitality during his stay in Prague in September 1998. The authors gratefully acknowledge financial support by the Grant Agency of the Czech Republic under the grant No. 205/97/0699 and support by the grant project of the Academy of Sciences of the Czech Republic No. K1-003-601/4.

## References

- Bisnovatyi-Kogan G.S., Silich S.A., 1995 *Rev. Mod. Phys.* 67, 661
- Blaauw A., 1961, *Bull. Astron. Inst. Netherlands* 15, 265
- Blinnikov S. I., Postnov K. A., 1998, *MNRAS* 293, L29
- Blitz L., Spergel D. N., Teuben P. J., et al., 1999, *ApJ* 514, 818
- Böhringer H., Hensler G., 1989, *A& A* 215, 147
- Brinks E., Bajaja E., 1986, *A& A* 169, 14
- Chevalier R. A., 1974, *ApJ* 188, 501
- Chevalier R. A. & Li Z.-Y., 1999, *ApJ Lett.* 520, L29
- Deul E. R., den Hartog R. H., 1990, *A& A* 229, 362
- Efremov Yu. N., 1998, in *Modern Problems of Stellar Evolution*, ed. D. S. Wiebe, Moscow, Geos, p. 37
- Efremov Yu. N., 1999a, *Astron. Lett.* 25, 74
- Efremov Yu. N., 1999b, *Astron. Rep.* 43, 284
- Efremov Yu. N., Elmegreen B. G., 1998a, *MNRAS* 299, 643
- Efremov Yu. N., Elmegreen B. G., 1998b, *IAU Symp.* 190, in press, (preprint astro-ph/9811216)
- Efremov Yu. N., Elmegreen B. G., Hodge P. W., 1998, *ApJ* 501, L163
- Ehlerová S., Palouš J., Theis Ch., Hensler G., 1997, *A&A* 328, 121
- Elmegreen B. G., 1994, *ApJ* 427, 384
- Hodge P. W., 1967, *PASP* 79, 29
- Kim S., 1998, PhD thesis, The Australian National University
- Kim S., Staveley-Smith L., Dopita M. A., et al., 1998, *ApJ* 503, 674
- Kroupa P., Bastian U., 1997, *New Astronomy* 2, 77
- Kulkarni S. R., Djorgovski S. G., Ramaprakash A. N., et al., 1998, *Nature* 393, 35
- Kulkarni S. R., Djorgovski S. G., Odewahn S. C., et al., 1999, *Nature* 398, 389
- Larsen S. S., Richtler T., 1999, *A&A* 345, 59
- Lipunov V. M., Postnov K. A., Prokhorov M. E., 1997, *MNRAS* 288, 245
- Loeb A., Perna R., 1998, *ApJ* 503, L35
- Lucke P. B., Hodge P. W., 1970, *AJ* 75, 171
- Luks Th., Rohlfs K., 1992, *A&A* 263, 41
- Mac Low M.-M., McCray R., 1988, *ApJ* 324, 776
- Ostriker J.P., Mc Kee C.F., 1988, *Rev. Mod. Phys.* 60, 1
- Palouš J., 1990, in *The Interstellar Disk-Halo Connection in Galaxies*, ed. H. Bloemen, Sterrewacht Leiden, The Netherlands, p. 101
- Paczynski B., 1998, *ApJ* 494, L45
- Rhode K. L., Saltzer J. J., Westpfahl D. J., Radice L. A., 1999, *AJ*, in press
- Schmutzler T., Tscharnuter W.M., 1993, *A& A* 273, 318
- Sedov L., 1959, *Similarity and Dimensional Methods in Mechanics*, Academy Press, New York
- Silich S. A., Tenorio-Tagle G., 1998, *MNRAS* 299, 249
- Silich S.A., Franco J., Palouš J., Tenorio-Tagle G., 1996, *ApJ* 468, 722
- Suchkov A. A., Balsara D. S., Heckman M., Leitherer C., 1994, *ApJ* 430, 511
- Tenorio-Tagle G., Palouš J., 1987, *A& A* 186, 287
- Tomisaka K., Ikeuchi S., 1988, *ApJ* 330, 695
- Vishniac E. T., 1994, *ApJ* 428, 186
- Wang Q. D., 1999, *ApJ* 517, L27
- Wijers R., 1998, *Nature* 393, 13